A Singlet Oxygen Priming Mechanism: Disentangling of

Photooxidative and Downstream Dark Effects

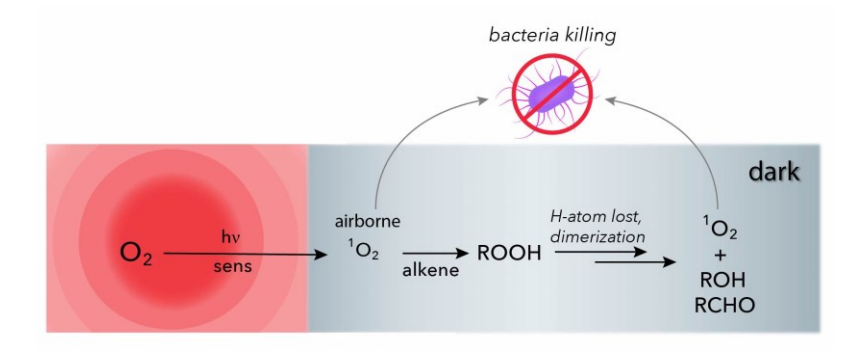
Shakeela Jabeen, 1,2 Maria Farag, 1 Belaid Malek, 1 Rajib Choudhury 3 and Alexander Greer 1,2*

¹ Department of Chemistry, Brooklyn College of the City University of New York, Brooklyn, New York 11210, United States

² Ph.D. Program in Chemistry, The Graduate Center of the City University of New York, 365 Fifth Avenue, New York, New York 10016, United States

Email address: agreer@brooklyn.cuny.edu

Table of contents graphic



³ Department of Chemistry, Arkansas Tech University, Russellville, AR 72801, United States

Abstract

Airborne singlet oxygen derived from photosensitization of triplet dioxygen is shown to react with an alkene surfactant (8-methylnon-7-ene-1 sulfonate) leading to 'ene' hydroperoxides that in the dark inactivate planktonic *E. coli*. The 'ene' hydroperoxide photoproducts are not toxic on their own, but they become toxic after the bacteria are pretreated with singlet oxygen. The total quenching rate constant (k_T) of singlet oxygen of the alkene surfactant was measured to be $1.1 \times 10^6 \text{ M}^{-1} \text{ s}^{-1}$ at the air/liquid interface. Through a new mechanism called singlet oxygen priming (SOP), the singlet oxygen toxin leads to the hydroperoxides then to peroxyl radicals, tetraoxide and decomposition products, which also disinfect, and therefore offer a "one two" punch. This offers a strong secondary toxic effect in an otherwise indiscernable dark reaction. The results provide insight to assisted killing by an exogenous alkene with dark toxicity effects following exposure from singlet oxygen.

Introduction

We present a study of a *photo*oxidation reaction that generates downstream (dark) peroxide species to inactivate bacteria. Previous reports have demonstrated that singlet oxygen (${}^{1}O_{2}$) can inactivate bacteria. ${}^{1-4}$ But a detailed study of ${}^{1}O_{2}$ inactivation of bacteria and latent dark toxicity of peroxide reaction products has not yet appeared. In this report, airborne ${}^{1}O_{2}$ is shown to not only be toxic itself, but also prime *E. coli* killing. The priming is due to a surfactant 1

forming hydroperoxides **2** and **3** that lead to a dark toxicity based on a ${}^{1}\text{O}_{2}$ -pretreatment (Figure 1). What we uncover is an important secondary process, where propagation of oxidative species in the dark leads to better bacterial disinfection. Other researchers have demonstrated important possibilities of dual acting compounds, ${}^{5\text{-}8}$ but provide little information about tandem light and dark toxic processes as they are not easily untangled.

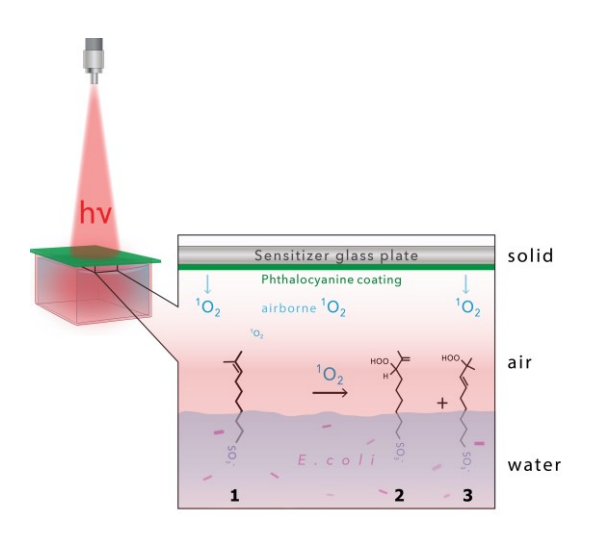


Figure 1. Our photoreactor is a triphasic system which segregates a phthalocyanine sensitizer from the generated airborne ${}^{1}O_{2}$. The sensitizer remains on the upper solid layer and is not in contact with the lower layer of water. Airborne ${}^{1}O_{2}$ was formed and traveled a ~ 0.5 mm distance to a solution of surfactant 1 and *E. coli*. The photoreaction kills *E. coli* and primes other *E. coli*, where otherwise harmless hydroperoxides 2 and 3 cause additional *E. coli* death in the dark.

Figure 2 shows a schematic of our reaction system. Reactive oxygen species (ROS) are formed *photochemically* in nanoseconds to microseconds by type I (oxygen radicals and radical

ions) and type II (singlet oxygen) sensitized oxidation processes. 9,10 The 'ene' hydroperoxide products serve as fingerprints for the existence of $^{1}O_{2}$ and have *dark* stabilities in the milliseconds to minutes time range. Thus, we hypothesized that light/dark toxicity processes can be disentangled, with properly designed experiments. This premise of this paper is that the field of aerobic photochemistry can benefit from tools able to decipher downstream dark reactions that follow initial photooxidative events.

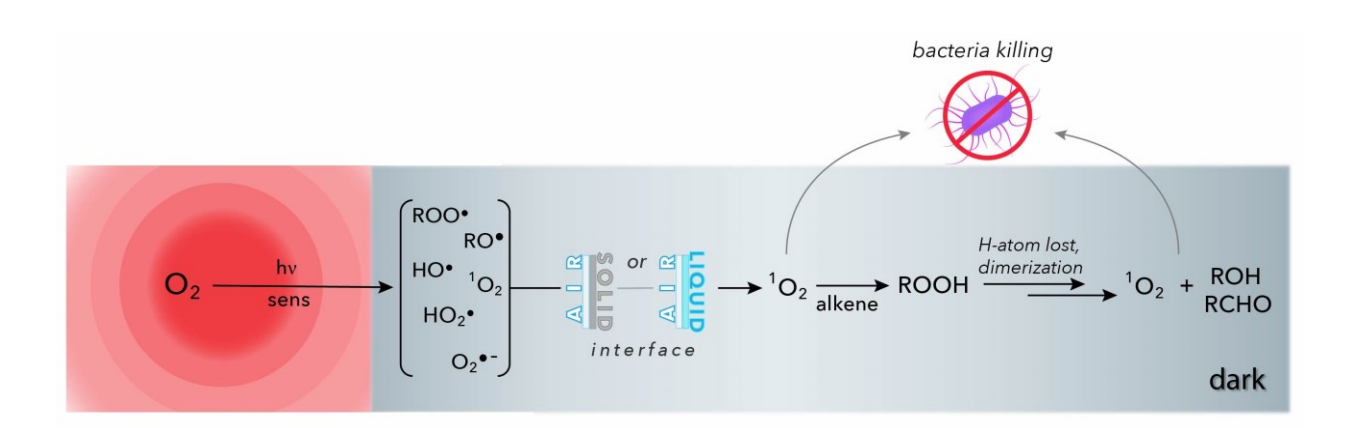


Figure 2. Schematic showing that complementary light and dark reactions arise in *separable* processes. We focus on light-dependent reaction of airborne ${}^{1}O_{2}$, and light-<u>in</u>dependent reaction of hydroperoxides (ROOH), but gloss over chemiluminescence and secondary excited-state processes.

We believe this premise has merit based on preliminary reports of damaging secondary dark reactions following photodynamic treatment.^{11,12} Previous work has shown the existence of oxidation products bearing toxicity competitive to their photogenerated ROS precursors. The process is illustrated in Figure 3. The first, light-dependent step (Figure 3a) produces cholesterol

hydroperoxides from type I and type II processes.¹¹ These cholesterol hydroperoxides can be stable for minutes. In Figure 3b, the second step is cytotoxic and *light-independent*. Other reports have also pointed to dark events in photochemical ¹³⁻¹⁶ and photobiological processes.¹⁷ Thus, the light/dark intersecting line is in further need of probing, and is the subject of this paper.

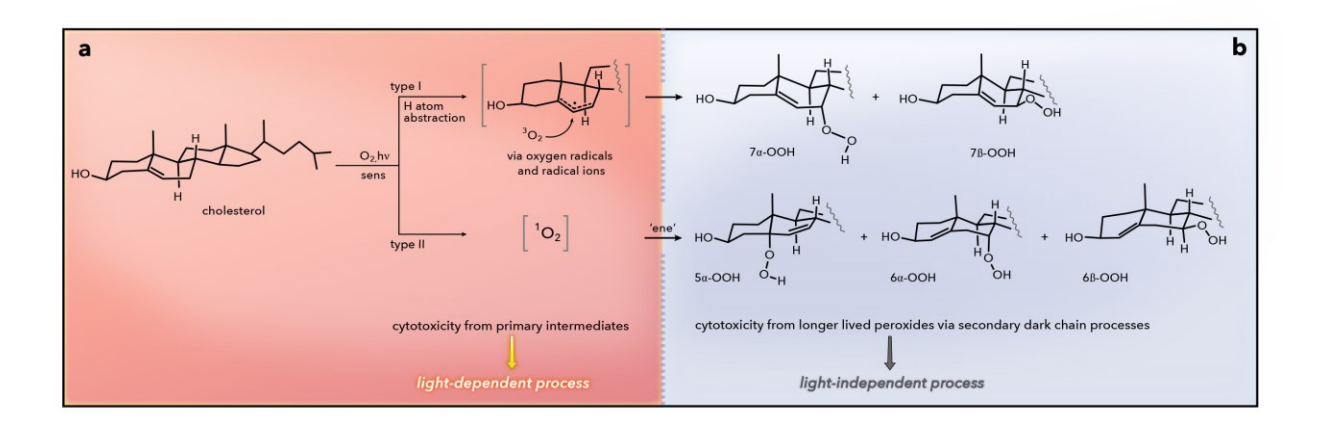


Figure 3. Secondary dark reactions following photodynamic treatment are damaging.¹¹ The product cholesterol hydroperoxides are important in the dark cytotoxicity.

But first, we note that the challenges in deducing the role of photogenerated ROS from downstream toxic species may be alleviated by the use of interfacial techniques. Figure 4 shows that interfacial techniques can enable some "control" over reactive oxygen intermediates. ROS in homogeneous media are formed in a mixture where downstream species are often difficult to discern (Figure 4a). In contrast, ${}^{1}O_{2}$ can be generated as a pure airborne species without the other ROS so that its toxicity can be tested with no ambiguity to the analysis. There are also reports of the arrival of other gaseous ROS to solid and liquid surfaces such as hydroxyl radicals

(Figure 4b)^{19,20} and emergence of species in porous and 2-phase media to help control oxidative reactivity and selectivity (Figure 4c).²¹⁻²⁴

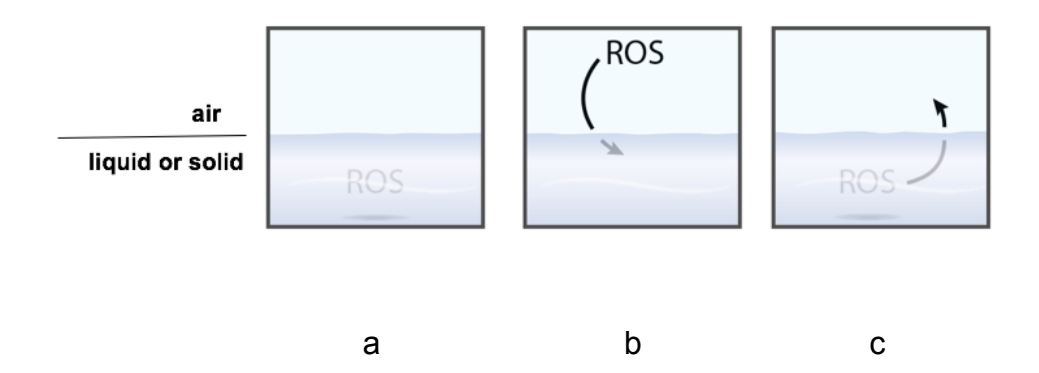


Figure 4. Scheme of homogeneous and interfacial techniques. (a) ROS in homogeneous solution, (b) arrival of ROS to a surface, and (c) emergence of ROS from a surface.

The methodology that we use is an offshoot of the interfacial technique in Figure 4b. Here, we report on generating airborne ${}^{1}O_{2}$ (${}^{1}\Delta_{g}$) in a pure form and capturing it on a second (liquid) surface. Our reactor enables for airborne ${}^{1}O_{2}$ delivery to a water surface bearing a monolayer of prenylsurfactant [(CH₃)₂C=CH(CH₂)₆SO₃⁻ Na⁺] (adjuvant) molecules, which initially form 'ene' hydroperoxides. The formation of airborne ${}^{1}O_{2}$ from a solid surface and subsequent interaction with the prenylsurfactant is shown in Figure 5. One objective was also to determine how efficiently prenylsurfactant 1 removes airborne ${}^{1}O_{2}$ at the air-liquid interface. What is key is that the sensitizer is physically separated from the water phase so that effects from direct sensitizer interactions and type I sensitized formation of oxygen radicals and radical ions can be discerned easily.

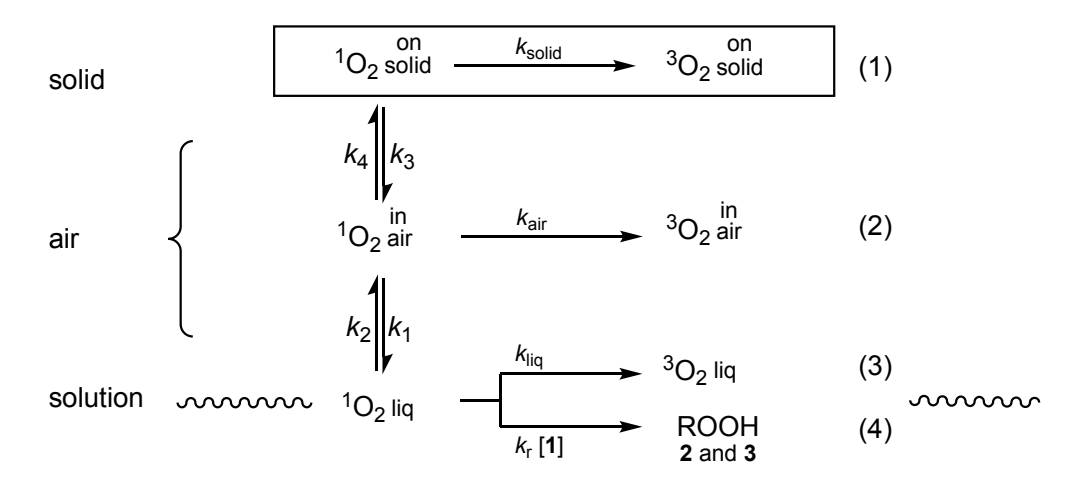


Figure 5. Scheme showing the formation of ${}^{1}O_{2}$ at the solid sensitizer and its physical quenching (eq 1), diffusion through air and physical quenching in air (eq 2) and by the liquid (eq 3), and chemical reaction with prenylsurfactant 1 to form hydroperoxides 2 and 3 (eq 4).

Thus, our reactor design in Figures 1 and 5 is similar to previous reports^{25,26} and reminiscent of 3-phase apparatuses to study airborne or interfacial ${}^{1}O_{2}{}^{27-29}$ and ROS^{30-33} and examine surfactant effects in disinfection, 34,35 but now it enables us to sort out the light/dark killing operations and the direct interaction of ${}^{1}O_{2}$ with the prenylsurfactant. Our hypothesis was that the formed hydroperoxides will be key to a dark killing process that temporarily lags behind the photochemical process. The stepwise delivery, with the first step being airborne ${}^{1}O_{2}$ and the second step hydroperoxides 2 and 3 with ${}^{1}O_{2}$ -pretreated microbe cells is found to be more effective at inactivating bacteria than each individually.

Results and Discussion

The reactor generates ¹O₂, which is delivered as a gas from a solid upper sensitizer plate to a water layer. An air space between the sensitizer plate and the water layer is bridged before ¹O₂ reaches the liquid for surfactant oxidation. This prenylsurfactant 1 provided us with the first opportunity to measure the interfacial effect on the total quenching rate constant (k_T) of 1O_2 . Two decay components were observed in the 1270 nm phosphorescence, a slow decay component attributed to ¹O₂ in the air gap and a fast decay component attributed to ¹O₂ at the air/D₂O interface. The fast component for the lifetime of singlet oxygen (τ_{Δ}) at the air/D₂O interface decreased on going from 48.0 µs (absence of 1) to 36.9 µs (with 5 mM 1). Addition of SDS (5 mM) led to a τ_{Δ} of ~48 μs as a result of the displacement of 1 (1 mM) at the interface. The measured τ_{Δ} is lower than the literature value of τ_{Δ} solvated in $D_2O~(66~\mu s)^{36}$ and implies a contribution of humidity. Thus, the surfactant quenching of the phosphorescence of ¹O₂ at the air/D₂O interface led to a $k_{\rm T}$ of 1.1 × 10⁶ M⁻¹ s⁻¹ (Figure S1, Supporting Information), and is inline with $k_{\rm T}$ values of trisubstituted alkenes in homogeneous organic solvents. ^{37,38} The kinetic derivation for this interfacial k_{T} measurement is located in the Supporting Information. We find that the prenylsurfactant 1 reacts with ¹O₂ to give two 'ene' products 7-hydroperoxy-8methylnon-8-ene-1-sulfonate 2 and (E)-8-hydroperoxy-8-methylnon-6-ene-1-sulfonate 3 in a 4:1 mixture of 2:3. Contribution of physical and chemical quenching of ¹O₂ by 1 and hydroperoxides 2 and 3 at the air/water interface were not determined. Similar to reports of ¹O₂ 'ene' reactions, 10,18,39 hydroperoxides 2 and 3 were detected in solution, but not products suggesting tandem ¹O₂ reactions, although the presence of iron and copper reductants found in bacteria are likely key to hydroperoxide decomposition, as we discuss in the Mechanism section later. Next,

our analysis shows the stepwise light and dark effects in E. coli killing that were previously unidentified. Similar to the time-resolved result, when SDS is added, the reactivity of 1 with ${}^{1}O_{2}$ appears to vanish with no detection of 2 and 3, which is consistent with displacement of 1 by the SDS at the interface.

Next, we focus on control experiments. We show that *E. coli* killing is minimal by light alone, surfactant **1** alone, or by hydroperoxides **2** and **3** alone in the dark. For example, when 50 μg/mL and 15 μg/mL *E. coli* was exposed to 669 nm light alone, killing of 4% and 8% was observed, respectively. When 15 μg/mL *E. coli* was exposed to surfactant **1** (1 mM) alone in the dark, only 2% killing was observed. When 15 μg/mL *E. coli* was exposed to a 4:1 mixture of **2** (0.144 M) and **3** (0.036 M) in the dark, 6% killing was observed. When simply left in the dark, 1.5% killing of *E. coli* was observed. The above control reactions demonstrate that there is low percent *E. coli* killing (2%) with light alone, or surfactant alone or hydroperoxides **2** and **3** alone in the dark.

In contrast to the control reactions, we have now identified dark contributions are significant *following* ${}^{1}O_{2}$ priming. The percent killing by airborne ${}^{1}O_{2}$ alone (Figure 6A, red bars) and the percent killing by *subsequent* exposure to hydroperoxides **2** and **3** in the dark (Figure 6A, grey bars) are plotted as a function of time. Exposure of *E. coli* (50 μg/mL) to airborne ${}^{1}O_{2}$ alone led to killing of $10\pm2\%$, $16\pm3\%$, $21\pm2\%$, $26\pm3\%$, $27\pm5\%$ after reaction times of 10 min (red bar, 1^{st} column), 20 min (red bar, 2^{nd} column), 30 min (red bar, 3^{rd} column), 45 min (red bar, 4^{th} column), and 60 min (red bar, 5^{th} column), respectively.

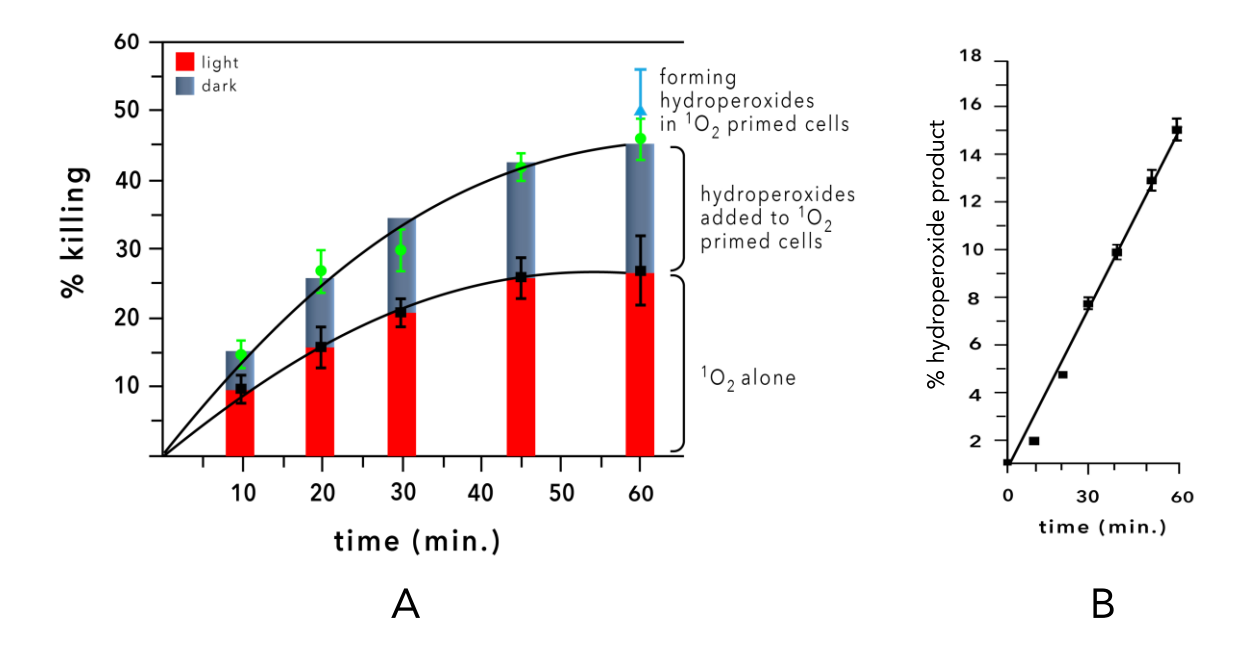


Figure 6. Percent *E. coli* killed by airborne ${}^{1}O_{2}$ alone (red bars) and the additional percent *E. coli* killed upon adding hydroperoxides in the dark as a follow-up treatment (grey bars). Exposure of *E. coli* to airborne ${}^{1}O_{2}$ alone for 10 min (red bar, 1^{st} column), 20 min (red bar, 2^{nd} column), 30 min (red bar, 3^{rd} column), 45 min (red bar, 4^{th} column), and 60 min (red bar, 5^{th} column), respectively. Hydroperoxides 2 and 3 were added in the dark in 4:1 ratios to airborne ${}^{1}O_{2}$ pretreated *E. coli* in concentrations of 0.01 mM after 10 min (grey bar, 1^{st} column), 0.03 mM after 20 min (grey bar, 2^{nd} column), 0.08 mM after 30 min (grey bar, 3^{rd} column), 0.12 mM after 45 min (grey bar, 4^{th} column), and 0.15 mM after 60 min (grey bar, 5^{th} column), where additional killing was observed. Three separate locations on the plate were used for the bacterial colony counting and the error was $\pm 2\%$. (B) This plots displays the steady generation of hydroperoxides 2 and 3 over time due to the reaction of airborne ${}^{1}O_{2}$ with surfactant 1 (1.0 mM).

The grey bars in Figure 6 show the share of the killing from the hydroperoxides following the airborne ${}^{1}O_{2}$ reaction. When these airborne ${}^{1}O_{2}$ -treated $E.\ coli$ were subsequently exposed to hydroperoxides **2** and **3** in the dark (in concentrations of 0.01, 0.03, 0.08, 0.12, and 0.15 mM), an additional 5±2% (grey bar, 1st column), 11±3% (grey bar, 2nd column), 9±3% (grey bar, 3rd column), 16±2% (grey bar, 4th column), and 19±3% (grey bar, 5th column) killing was observed, respectively. By comparison, when airborne ${}^{1}O_{2}$ -treated $E.\ coli$ were subsequently exposed to surfactant **1** (1 mM) in the dark, no additional killing was observed. Thus, we show that the $E.\ coli$ killing relates to both airborne ${}^{1}O_{2}$ and to hydroperoxides **2** and **3** with ${}^{1}O_{2}$ -pretreated cells.

As we will see next, hydroperoxides **2** and **3** are formed by a reaction of airborne ${}^{1}O_{2}$ with surfactant **1** and have a similar priming effect. We also show that the toxicity to airborne ${}^{1}O_{2}$ led to enhanced killing with the generation of the hydroperoxides *in situ*. As we noted above, the reaction of airborne ${}^{1}O_{2}$ with surfactant **1** leads to hydroperoxides **2** and **3**, which amplify *E. coli* killing by 1.7 to 2-fold by comparison to airborne ${}^{1}O_{2}$ in the absence of **1**. Figure 6B shows that over the photolysis time of 10 min to 60 min, a H₂O solution of 1.0 mM surfactant **1** formed 0.02 mM up to 0.18 mM of hydroperoxides **2** and **3**. The surfactant **1** conversion to hydroperoxides **2** and **3** was increased over time, which enhanced the *E. coli* killing by ${}^{1}O_{2}$. Airborne ${}^{1}O_{2}$ with surfactant **1** forming **2** and **3** yielded 50% killing, which is higher than that by **1** alone (2.6%) or by airborne ${}^{1}O_{2}$ alone (25%) (Figure 6A, red bar, 5th column); the latter two add up to only 27.6%, not the 46%.

Thus, whether the hydroperoxides are generated *in situ* or added after the treatment of airborne ${}^{1}O_{2}$, our data show that the hydroperoxides cause a heightened *E. coli* killing by ${}^{1}O_{2}$. Namely, adding hydroperoxides 2 and 3 (0.15 mM) in the dark after treatment with airborne ${}^{1}O_{2}$

for 1 h led to a similar inactivation of 50 μ g/mL *E. coli* (46%) when compared to airborne $^{1}O_{2}$ with surfactant 1 (50%). Furthermore, we probed the stabilities of hydroperoxides 2 and 3 in terms of their decomposition rates in DMSO. We found that 2 is more stable than 3 under various conditions. Hydroperoxide 2 is less stable since it decomposes after 1 h at 100 °C in DMSO, whereas hydroperoxide 3 required heating at 185 °C for 2 h. In contrast, the presence of *E. coli* decreased the stability of both hydroperoxides to several minutes suggesting that they reacted with the bacteria. Although NMR analysis did not discern whether 3 was presevered for a longer period than 2 in the presence of the bacteria, their degradation was shown likely after reaction with Fe²⁺ has occurred, and not observed under normal iron free conditions in DMSO.

We find a relationship between killing increase and added hydroperoxides **2** and **3** after the bacteria were exposed to airborne ${}^{1}O_{2}$ (Figure 7A). The figure shows a near linear killing. There was a steady increase but no clear induction required for the buildup of hydroperoxides **2** and **3**. The dark contribution leads to additional killing, in which the enhancement to the dark toxicity comes after ${}^{1}O_{2}$ "priming" via H-abstraction and radical chain processes as a separate stressing route than only peroxidation from airborne ${}^{1}O_{2}$ (Figure 7B), as we elaborate on below. Namely, how do the hydroperoxides enhance the *E. coli* killing from ${}^{1}O_{2}$ -primed microbe cells? There is a seemingly important potentiation of the bacterial killing in the dark process following the light process. By itself, this dark process is not effective in the killing. Why? A mechanistic analysis that is shown below provides possible answers.

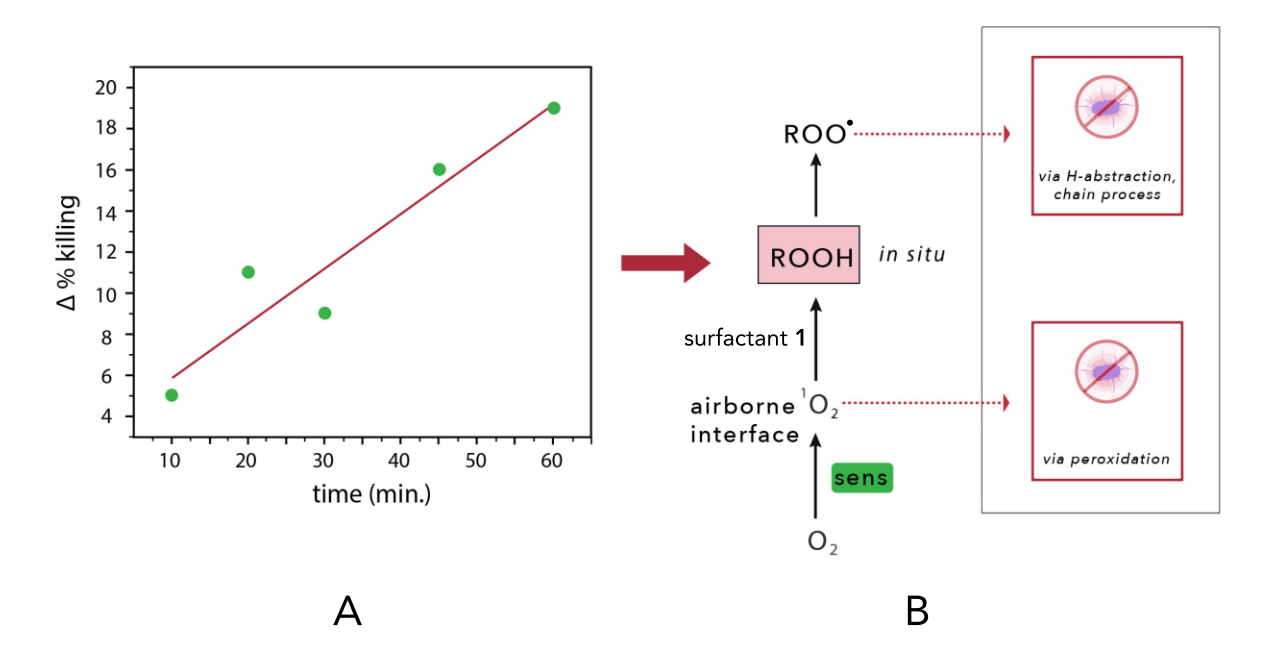


Figure 7. The dark process at work. (A) This is the difference between the percent killing by airborne ${}^{1}O_{2}$ alone and with added hydroperoxides after the bacteria were exposed to airborne ${}^{1}O_{2}$. (B) This proposed mechanism accounts for how the hydroperoxides do more work, where the airborne ${}^{1}O_{2}$ and the hydroperoxides are not solo acts. The *E. coli* killing takes place by preexposure to airborne ${}^{1}O_{2}$ (peroxidation), in which a postreaction with hydroperoxides 2 and 3 provokes more killing by H-abstraction and radical chain processes.

Mechanism

We posit three mechanisms: (1) reactive species formed in the decomposition of the hydroperoxides, (2) exogenous alkene molecules assisting in the *E. coli* oxidative stress, and (3) singlet oxygen priming (SOP) as distinct from the known photodynamic priming (PDP).

(1) Secondary species are produced upon the decomposition of the primary photoperoxides 2 and 3 (Figure 8). *Path A:* For hydroperoxide 2 but not 3, tetraoxide formation

and Russell cyclization and decomposition 40-42 can lead to 3-methyl enone 4 and enol 5, where the dark cleavage forms excited-state 4 with energy transfer to ${}^3{\rm O}_2$ for additional ${}^1{\rm O}_2$. A rapid decomposition of tetraoxide from the 2° hydroperoxide 2 is expected compared to the 3° hydroperoxide 3, which is consistent with the greater observed stability of 2 than 3. Path B: For hydroperoxide 2 but not 3, tetraoxide formation and decomposition can lead to hydrotrioxide 6 and 3-methyl enone 4. The formation of 4 and 6 arising from the loss of a hydrogen atom from 2 via 2(-H•) seems plausible. A previous DFT study⁴² has identified low-energy dimerization behavior of peroxy radicals to hydrotrioxide with a 12.3 kcal/mol saddle point. Avzyanova et al. 43 and Plesničar et al. 44,45 have reported on the synthesis of organic hydrotrioxides, which like other peroxide decompositions can be accompanied by ¹O₂ formation. ^{39,46} Paths C and E: The Hock rearrangement can arise by proton transfer to 2 and 3 leading to water adducts 2(+H⁺) and 3(+H⁺). The conversion of the 3(+H⁺) to cation 12 and water would lead to the 3° hydroperoxide rearrangement, which is easier than the 2° hydroperoxide rearrangement. This is contraty to our results due to the observed stability of hydroperoxides 2 and 3 at pH 4.5 for 1 h. This is also contrary to the stabilities that we observe for 2 and 3, namely lower stability of a more substituted carbocation, although the Hock reaction can lead to toxic aldehydes. 47,48 Path D: For 3, the dimerization of 2 moles of $3(-H^{\bullet})$ can reach tetraoxide, and decompose to O_2 and alkoxy radical 10 with subsequent loss of CH₃• and formation of enone 11. Lastly, we have evidence that once formed, hydroperoxides 2 and 3 are not involved in an interconversion with each other by HOO• radical migration (Schenck reaction), thus ruling it out as the origin of dark toxicity. 49-Two further candidate mechanisms, include a photopriming effect to deplete cellular antioxidants, thereby accentuating secondary ROS effects post-¹O₂ exposure. Also, the initial ¹O₂

may result in leakage of Fe²⁺, which could persist to facilitate decomposition of the hydroperoxides to generate subsequent ROS.

A Russell RHO
$$\stackrel{\longrightarrow}{}_{0}$$
 R $\stackrel{\longrightarrow}{}_{0}$ R $\stackrel{\longrightarrow}{$

Figure 8. Paths A-E show reactive intermediates that are potentially formed after the initial reaction of prenylsurfactant $\mathbf{1}$ [(CH₃)₂C=CH(CH₂)₆SO₃⁻ Na⁺] with airborne 1 O₂. In the figure R = (CH₂)₅SO₃⁻.

(2) Bacteria pre-exposure to airborne ${}^{1}O_{2}$ is shown to enhance the killing of hydroperoxides **2** and **3** in the dark, where we consider the prenylsurfactant's function as an exogenous alkene. Prenylsurfactant **1** (1 mM in 0.6 mL H₂O, 3.6×10^{17} molecules) is considered as an exogenous alkene source supplementing endogenous alkene sites in the bacteria based on total unsaturated alkene content. Lipids are the primary source of endogenous alkenes, in which

lipid hydroperoxides are readily formed. Sec. Biological targets for ${}^{1}O_{2}$ also include sites in proteins and DNA. The number of surfactant alkenes and unsaturated fatty acid sites per gram of bacterial dry weight in E. $coli^{60,61}$ in our experiments is a ratio of \sim 400:1 (exogenous-to-endogenous unsaturated sites). Thus, dissolution of hydroperoxides 2 and 3 into water is proposed to take place, where post- ${}^{1}O_{2}$ (i.e., ROOH) exogenous and endogenous hydroperoxides release "oxidative storage" for dark killing with hydroperoxide decomposition and formation of toxic byproducts. Next, we elaborate on the issue of exogenous species or adjuvants as the origin of the boost in photokilling as a mechanistic subject.

(3) Airborne ¹O₂ followed secondarily by ROS from hydroperoxide decomposition can be regarded as singlet oxygen priming (SOP) (Figure 9A). The enhanced *E. coli* killing with the surfactant hydroperoxides in Figure 6 is a special example of a post ¹O₂-stressing process. If we adopt this view, we conclude that SOP (Figure 9A) is now distinguishiable from "photodynamic priming" (PDP) (Figure 9B).⁶²⁻⁶⁵ Mayten and Hasan⁶² pioneered the concept of PDP, which is an adjuvant pretreatment in the dark to improve not only fluorescent imaging but also the cells' susceptibility to photosensitized killing. In the case of PDP, adjuvant compounds such as irinotecan, methotrexate, 5-fluorouracil, vitamin D and derivatives lead to an amplified effect in PDT. The mechanism of PDP includes enhanced conversion of exogenous ALA, and thus increased protoporphyrin IX concentrations via exogenous ALA additions to cells, for enhanced killing.

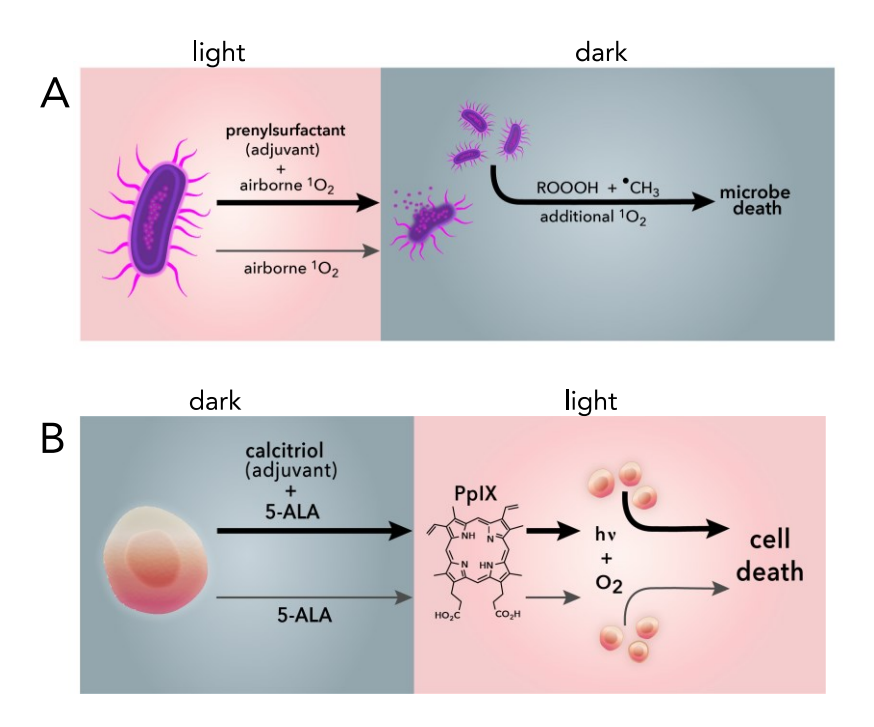


Figure 9. (A) Singlet oxygen priming (SOP) that enhances microbe inactivation by initial exposure to airborne ${}^{1}O_{2}$. It is proposed that the exogenous alkene (prenylsurfactant) converts to hydroperoxide (with -H• via Fe²⁺) and on the basis of peroxyl radical dimerization is expected to form hydrotrioxide, CH₃•, and additional ${}^{1}O_{2}$ to account for the dark toxicity. (B) Photodynamic priming (PDP) in which adjuvants such as calcitriol are used for the enhancement of ALA-based photodynamic therapy (PDT).

In summary, our data show a significant increase in the bacteria killing by airborne ${}^{1}O_{2}$ as the concentration of hydroperoxides **2** and **3** is increased. This leads to a new proposed path in which the airborne ${}^{1}O_{2}$ is toxic to and primes other bacteria. In choosing the most likely mechanism to account for the dark killing, peroxyl radical dimerization to tetraoxide is envisaged to lead to ${}^{1}O_{2}$ (path A), hydrotrioxide **6** (path B), and CH₃• radicals (path D). Of note, hydrotrioxide **6** is expected to readily decompose and taking advantage of their toxicity due to

the oxidation power they carry is yet to be realized in the literature. Our control data are not consistent with the Hock rearrangment to carbocations and aldehydes (paths C and E), or the Schenck rearrangement of HOO• radical. Furthermore, both exogenous to endogenous alkene groups in the *E. coli* samples contribute to secondary oxidative stress by their peroxide buildup in terms of dark killing.

Conclusion

We were surprised to discover how significant the dark process was in terms of E. coli killing in the post-photochemical reaction. The analysis shows that E. coli is stable to light alone and stable to the hydroperoxides $\mathbf{2}$ and $\mathbf{3}$ alone. However, the observed dark killing by the hydroperoxides increases only after ${}^{1}O_{2}$ priming.

Until now, the state of the art was to kill cells and microbes via tuning of sensitizer structure, which is a common benchmark in this field. 66-68 Our results help to dissect a key dark reaction following an initial ${}^{1}\text{O}_{2}$ photoreaction. New context is provided where we now understand separate processes that are usually studied as blended. We also understand a distinction between SOP vs PDP. SOP is envisioned to fit in microbe inactivation, whereas PDP increases cell eradication mainly from higher local sensitizer concentrations. The remaining challenges are to measure chemiluminescence from thermal peroxide cleavage and to deduce relative contributions of reactive species in the secondary dark reaction to enable further increases in the dark killing component.

Experimental Section

General Aspects. Frontier Scientific, Inc. supplied the aluminum (III) phthalocyanine chloride tetrasulfonic acid. Sigma-Aldrich supplied the benzoic acid, sodium dodecyl sulfate (SDS), DMSO- d_6 , and D₂O. A U.S. Filter Corporation deionization system was used to purify H₂O. Mutant of *E. coli* K₁₂ (strain CW 3747) was used. A thin piece of Corning 7930 porous Vycor glass (PVG) sized 1.0 mm × 2.25 cm² was used. Surfactant 8-methylnon-7-ene-1 sulfonate 1 was synthesized as reported in the literature. ²⁶ 7-Hydroperoxy-8-methylnon-8-ene-1-sulfonate anion 2 and (*E*)-8-hydroperoxy-8-methylnon-6-ene-1-sulfonate anion 3 were isolated from the reaction mixture by evaporating water with flowing nitrogen gas over the sample, and the residue was dissolved in DMSO- d_6 and analyzed by NMR. Hydroperoxides 2 and 3 are difficult to purify due to their lability on silica; we were unable to purify one from the other due to similarities in polarities. An instrument was used to collect NMR data at 400 MHz (1 H) and 100.6 MHz (13 C). A Hitachi UV-vis U-2001 instrument was used to collect UV-vis data. A digital pyrometer was used to measure water temperatures.

Photoreactor and Airborne Singlet Oxygenations. A quartz cuvette sized $1.0 \text{ cm}^2 \times 0.7 \text{ cm}$ containing surfactant **1** in the presence or absence of *E. coli* in 0.60 mL H₂O or D₂O was used, where the PVG lid [square $(2.25 \text{ cm}^2 \times 1.0 \text{ mm})$] was placed on top. The lid's bottom face was coated with 1.1×10^{-5} mol aluminum (III) phthalocyanine chloride tetrasulfonic acid per gram PVG. This lid was not in contact with the water. From the sensitizer plate to the water surface, airborne ${}^{1}\text{O}_{2}$ traversed a distance of 0.4 mm near the walls of the cuvette up to 1.5 mm in the middle of the meniscus. Careful analysis showed that no phthalocyanine became separated from the sensitizing glass or was relocated in the water. Time-resolved experiments were carried out. Namely, the total quenching rate constant (k_{T}) for the reaction of airborne ${}^{1}\text{O}_{2}$ with **1** was determined at room temperature by irradiating the sensitizer plate with 355-nm light from a

Surelite MiniliteTM pulsed Nd:YAG laser (Continuum©) and monitoring the 1270 nm phosphorescence of ¹O₂ with a photomultiplier tube (H10330A-45, Hamamatsu Corp.). The 1270 nm light from ¹O₂ was filtered through a 1250 nm long-pass and a 1270 nm band-pass filter before reaching the photomultiplier tube. The amount of 1 used ranged from 5- to 20-fold less (for the time-resolved experiments) and 10-fold less (for the bacterial experiments) than its reported critical micellar concentration (CMC) of 9.7 mM.²⁶ Planktonic bacteria were illuminated by a diode laser (model 7404, Intense, Inc.) of 669-nm light (383 mW), passing first through an FT-400-EMT optical fiber (Thorlabs, Newton NJ), and second through the PVG sensitizer plate generating airborne ¹O₂ on its bottom side, which diffused through air and reaching the aqueous solution containing the bacteria. The end of the fiber tip was located 3.0 cm above the PVG lid. The sensitizer plate contained a strong absorption in the 355-nm region and in the 669-nm region to overlap well with the YAG and diode lasers. The incident photons arrived in a Gaussian distribution to the sensitizer plate. The temperature of the water in the apparatus was found to increase by ~3.5 °C over an irradiation period of 1 h with the 669-nm laser light. Airborne ¹O₂ emerged from the phthalocyanine plate and descended downward through an air gap to the water later.

E. coli Inactivation. Inactivation data were collected with the photoreactor, in which *E. coli* was used in amounts of 15 μg/mL and 50 μg/mL from quantitation with UV-VIS. The 3-phase apparatus in Figure 1 was used to react airborne ${}^{1}O_{2}$ with *E. coli*. After the reaction, a portion of the solution (0.1 mL) was placed onto agar plates, and was incubated at 37 °C for 24 h to quantitate the number of colonies. To assess the dark toxicity, we exposed *E. coli* to 1 at a concentration of 1 mM as well as hydroperoxides 2 and 3 at concentrations of 0.01 up to 0.2 mM in 4:1 ratios. A commercial *Bac*Light viability kit was used for LIVE/DEAD assays, which

contained SYTO-9 and propidium iodide. After centrifuging, *E. coli* samples were exposed to the SYTO-9 and propidium iodide for 15 min at 37 °C, and then analyzed with a fluorescence microscope.

Supporting Information

The Supporting Information is available free of charge: Estimation of endogenous alkene in bacteria, kinetic derivagtioon, plot of k_{obs} (s⁻¹) vs [prenylsurfactant 1] (M).

Acknowledgments. We acknowledge support from the National Science Foundation (CHE-1856765). We also thank Leda Lee for assistance with the graphic arts work.

ORCID

Alexander Greer https://orcid.org/0000-0003-4444-9099

References

- (1) Maisch, T. Strategies to Optimize Photosensitizers for Photodynamic Inactivation of Bacteria. *J. Photochem. Photobiol. B* **2015**, *150*, 2–10.
- (2) Cieplik, F.; Späth A.; Regensburger, J.; Gollmer, A.; Tabenski, L.; Hiller, K.-A.; Bäumler, W.; Maisch, T.; Schmalz, G. Photodynamic Biofilm Inactivation by SAPYR: An Exclusive Singlet Oxygen Photosensitizer. *Free Rad. Biol. Med.* **2013**, *65*, 477–487.

- (3) Maisch, T.; Baier, J.; Franz, B.; Maier, M.; Landthaler, M.; Szeimies, R.-M.; Bäumler, W. The Role of Singlet Oxygen and Oxygen Concentration in Photodynamic Inactivation of Bacteria. *Proc. Natl. Acad. Sci. USA* **2007**, *104*, 7223–7228.
- (4) Pushalkar, S.; Ghosh, G.; Xu, Q.; Liu, Y.; Ghogare, A. A.; Atem, C.; Greer, A.; Saxena, D.; Lyons, A. M. Superhydrophobic Photosensitizers: Airborne ¹O₂ Killing of an *In vitro* Oral Biofilm at the Plastron Interface. *ACS Appl. Mater. Interfaces* **2018**, *10*, 25819–25829.
- (5) Sgambellone, M. A.; David, A.; Garner, R. N.; Dunbar, K. R.; Turro, C. Cellular Toxicity Induced by the Photorelease of a Caged Bioactive Molecule: Design of a Potential Dual-Action Ru(II) Complex. *J. Am. Chem. Soc.* **2015**, *135*, 11274–11282.
- (6) Knoll, J. D.; Albani, B. A.; Turro, C. New Ru(II) Complexes for Dual Photoreactivity: Ligand Exchange and ¹O₂ Generation. *Acc. Chem. Res.* **2015**, *48*, 2280–2287.
- (7) Belh, S. J.; Walalawela, N.; Lekhtman, S.; Greer, A. Dark-binding Process Relevant to Preventing Photooxidative Damage: Conformation Dependent Light and Dark Mechanisms by a Dual-functioning Diketone. *ACS Omega* **2019**, *4*, 22623–22631.
- (8) Taylor, J. S. Biomolecules: The Dark Side of Sunlight and Melanoma. *Science* **2015**, *347*, 824.
- (9) Baptista, M. S.; Cadet, J.; Mascio, P. Di.; Ghogare, A. A.; Greer, A.; Hamblin, M. R.; Lorente, C.; Nunez, S. C.; Ribeiro, M. S.; Thomas, A. H.; Vignoni, M.; Yoshimura, T. M. Type I and II Photosensitized Oxidation Reactions: Guidelines and Mechanistic Pathways. *Photochem. Photobiol.* **2017**, *93*, 912–919.

- (10) Ghogare, A. A.; Greer, A. Using Singlet Oxygen to Synthesize Natural Products and Drugs. *Chem. Rev.* **2016**, *116*, 9994–10034.
- (11) Girotti, A. W.; Korytowski, W. Cholesterol Peroxidation as a Special Type of Lipid Oxidation in Photodynamic Systems. *Photochem. Photobiol.* **2019**, *95*, 73–82.
- (12) Chiemezie, C.; Greer, A. Secondary Dark Reactions Following Photodynamic Treatment Are More Damaging Than Previously Thought. *Photochem. Photobiol.* **2019**, *95*, 460–461.
- (13) Bartling, H.; Eisenhofer, A.; König, B.; Gschwind, R. M. The Photocatalyzed Aza-Henry Reaction of *N*-Aryltetrahydroisoquinolines: Comprehensive Mechanism, H• versus H⁺ Abstraction, and Background Reactions. *J. Am. Chem. Soc.* **2016**, *138*, 11860–11871.
- (14) Ji, Y.; DiRocco, D. A.; Kind, J.; Thiele, C. M.; Gschwind, R. M.; Reibarkh, M. LED-Illuminated NMR Spectroscopy: A Practical Tool for Mechanistic Studies of Photochemical Reactions. *ChemPhotoChem* **2019**, *3*, 984–992.
- (15) Nitschke, P.; Lokesh, N.; Gschwind, R. M. Combination of Illumination and High Resolution NMR Spectroscopy: Key Features and Practical Aspects, Photochemical Applications, and new Concepts. *Prog. Nucl. Mag. Res. Spect.* **2019**, *114-115*, 86–134.
- (16) Planas, O.; Boix-Garriga, E.; Rodríguez-Amigo, B.; Torra, J.; Bresolí-Obach, R.; Flors, C.; Viappiani, C.; Agut, M.; Ruiz-González, R.; Nonell, S. Chapter 9. Newest Approaches to Singlet Oxygen Photosensitisation in Biological Media. In *Photochemistry: Volume 42*; The Royal Society of Chemistry, 2015; Vol. 42, pp 233–278.

- (17) Robert, G.; Wagner, J. R. Tandem Lesions Arising from 5-(Uracilyl)Methyl Peroxyl Radical Addition to Guanine: Product Analysis and Mechanistic Studies. *Chem. Res. Toxicol.* **2020**, *33*, 565–575.
- (18) Clennan, E.; Pace, A. Advances in Singlet Oxygen Chemistry. *Tetrahedron* **2005**, *61*, 6665–6691.
- (19) Forbes, M. D. E. Radicals with Multiple Personalities. *Nat. Chem.* **2013**, *5*, 447–449.
- (20) D'Andrea, T. M.; Zhang, X.; Jochnowitz, E. B.; Lindeman, T. G.; Simpson, C. J. S. M.; David, D. E.; Curtiss, T. J.; Morris, J. R.; Ellison, G. B. Oxidation of Organic Films by Beams of Hydroxyl Radicals. *J. Phys. Chem. B* **2008**, *112*, 535–544.
- (21) Natarajan, A.; Kaanumalle, L. S.; Jockusch, S.; Gibb, C. L. D.; Gibb, B. C.; Turro, N. J.; Ramamurthy, V. Controlling Photoreactions with Restricted Spaces and Weak Intermolecular Forces: Exquisite Selectivity during Oxidation of Olefins by Singlet Oxygen. *J. Am. Chem. Soc.* **2007**, *129*, 4132–4133.
- (22) Uppili, S.; Shailaja, J.; Jayaraman, S.; Ramamurthy, V. Zeolite-Coated Quartz Fibers as Media for Photochemical and Photophysical Studies. *Chem. Commun.* **2002**, *6*, 596–597.
- (22) Macia, N.; Bresoli-Obach, R.; Nonell, S.; Heyne, B. Hybrid Silver Nanocubes for Improved Plasmon-Enhanced Singlet Oxygen Production and Inactivation of Bacteria. *J. Am. Chem. Soc.* **2019**, *141*, 684–692.

- (23) Turro, N. J. Fun with Photons, Reactive Intermediates, and Friends. Skating on the Edge of the Paradigms of Physical Organic Chemistry, Organic Supramolecular Photochemistry, and Spin Chemistry. *J. Org. Chem.* **2011**, *76*, 9863–9890.
- (24) Grandbois, M.; Latch, D. E.; McNeill, K. Microheterogeneous Concentrations of Singlet Oxygen in Natural Organic Matter Isolate Solutions. *Environ. Sci. Technol.* **2008**, *42*, 9184–9190.
- (25) Choudhury, R.; Greer, A. Synergism Between Airborne Singlet Oxygen and a Trisubstituted Olefin Sulfonate for the Inactivation of Bacteria. *Langmuir* **2014**, *30*, 3599–3605.
- (26) Malek, B.; Fang, W.; Abramova, I.; Walalawela, N.; Ghogare, A. A.; Greer, A. Ene Reactions of Singlet Oxygen at the Air-Water Interface. *J. Org. Chem.* **2016**, *81*, 6395–6401.
- (27) Naito, K.; Tachikawa, T.; Cui, S.-U.; Sugimoto, A.; Fujitsuka, M.; Majima, T. Single-Molecule Detection of Airborne Singlet Oxygen. *J. Am. Chem. Soc.* **2006**, *128*, 16430–16431.
- (28) Midden, W. R.; Wang, S. Y. Singlet Oxygen Generation for Solution Kinetics: Clean and Simple. *J. Am. Chem. Soc.* **1983**, *105*, 4129–4135.
- (29) Dahl, T. A.; Midden, W. R.; Hartman, P. E. Pure Singlet Oxygen Cytotoxicity for Bacteria. *Photochem. Photobiol.* **1987**, *46*, 345–352.
- (30) Naito, K.; Tachikawa, T.; Fujitsuka, M.; Majima, T. Real-time Single-molecule Imaging of the Spatial and Temporal Distribution of Reactive Oxygen Species with Fluorescent Probes: Applications to TiO₂ Photocatalysts. *J. Phys. Chem. C* **2008**, *112*, 1048–1059.

- (31) Zhang, X.; Barraza, K. M.; Upton, K. T.; Beauchamp, J. Time Resolved Study of Hydroxyl Radical Oxidation of Oleic Acid at the Air-Water Interface. *Chem. Phys. Lett.* **2017**, *683*, 76–82.
- (32) Zhang, X.; Barraza, K. M.; Beauchamp, J. L. Cholesterol Provides Nonsacrificial Protection of Membrane Lipids from Chemical Damage at Air–water Interface. *Proc. Natl. Acad. Sci. USA* **2018**, *115*, 3255–3260.
- (33) Kim, H. I.; Kim, H.; Shin, Y. S.; Beegle, L. W.; Jang, S. S.; Neidholdt, E. L.; Goddard, W. A.; Heath, J. R.; Kanik, I.; Beauchamp, J. L. Interfacial Reactions of Ozone with Surfactant Protein B in a Model Lung Surfactant System. *J. Am. Chem. Soc.* **2010**, *132*, 2254–2263.
- (34) Donabedian, P. L.; Creyer, M. N.; Monge, F. A.; Schanze, K. S.; Chi, E. Y.; Whitten, D. G. Detergent-Induced Self-Assembly and Controllable Photosensitizer Activity of Diester Phenylene Ethynylenes. *Proc. Natl. Acad. Sci. USA* **2017**, *114*, 7278–7282.
- (35) Hill, E. H.; Pappas, H. C.; Whitten, D. G. Activating the Antimicrobial Activity of an Anionic Singlet-Oxygen Sensitizer Through Surfactant Complexation. *Langmuir* **2014**, *30*, 5052–5056.
- (36) Bartusik, D.; Aebisher, D.; Lyons, A. M.; Greer, A. Bacterial Inactivation by a Singlet Oxygen Bubbler: Identifying Factors Controlling the Toxicity of ¹O₂ Bubbles. *Environ. Sci. Technol.* **2012**, *46*, 12098–12104.
- (37) Manring, L. E.; Foote, C. S. Chemistry of Singlet Oxygen. 44. Mechanism of Photooxidation of 2,5-Dimethylhexa-2,4-diene and 2-Methyl-2-pentene. *J. Am. Chem. Soc.* **1983**, *105*, 4710–4717.

- (38) Wilkinson, F.; Helman, W. P.; Ross, A. B. Quantum Yields for the Photosensitized Formation of the Lowest Electronically Excited Singlet State of Molecular Oxygen in Solution. *J. Phys. Chem. Ref. Data* **1995**, *22*, 663–1021.
- (39) Alberti, M. N.; Orfanopoulos, M. Unraveling the Mechanism of the Singlet Oxygen Ene Reaction: Recent Computational and Experimental Approaches. *Chem. Eur. J.* **2010**, *16*, 9414–9421.
- (40) Di Mascio, P.; Martinez, G. R.; Miyamoto, S.; Ronsein, G. E.; Medeiros, M. H. G.; Cadet, J. Singlet Molecular Oxygen Reactions with Nucleic Acids, Lipids, and Proteins. *Chem. Rev.* **2019**, *119*, 2043–2086.
- (41) Liang, Y.-N.; Li, J.; Wang, Q.-D.; Wang, F.; Li, X.-Y. Computational Study of the Reaction Mechanism of the Methylperoxy Self-reaction. *J. Phys. Chem. A* **2011**, *115*, 13534–13541.
- (42) Abramova, I.; Rudshteyn, B.; Liebman, J. F.; Greer, A. Computed Regioselectivity and Conjectured Biological Activity of Ene Reactions of Singlet Oxygen with the Natural Product Hyperforin. *Photochem. Photobiol.* **2017**, *93*, 626–631.
- (43) Avzyanova, E. V.; Timerghazin, Q. K.; Khalizov, A. F.; Khursan, S. L.; Spirikhin, L. V.; Shereshovets, V. V. Formation of Hydrotrioxides during Ozonation of Hydrocarbons on Silica Gel. Decomposition of Hydrotrioxides. *J. Phys. Org. Chem.* **2000**, *13*, 87–96.
- (44) Eržen, E.; Cerkovnik, J.; Plesničar B. Endo/ExoIsomerism in Norcarane and 2-Norcaranol Hydrotrioxides (ROOOH). *J. Org. Chem.* **2003**, *68*, 9129–9131.

- (45) Plesničar, B.; Cerkovnik, J.; Koller, J.; Kovac, F. Chemistry of Hydrotrioxides. Preparation, Characterization, and Reactivity of Dimethylphenylsilyl Hydrotrioxides. Hydrogen Trioxide (HOOOH), a Reactive Intermediate in Their Thermal Decomposition? *J. Am. Chem. Soc.* **1991**, *113*, 4946–4953.
- (46) Ghorai, P.; Dussault, P. H. A New Peroxide Fragmentation: Efficient Chemical Generation of ¹O₂ in Organic Media. *Org. Lett.* **2009**, *11*, 4572–4575.
- (47) Tasso, T. T.; Schlothauer, J. C.; Junqueira, H. C.; Matias, T. A.; Araki, K.; Liandra-Salvador, É.; Antonio, F. C. T.; Homem-de-Mello, P.; Baptista, M. S. Photobleaching Efficiency Parallels the Enhancement of Membrane Damage for Porphyrazine Photosensitizers. *J. Am. Chem. Soc.* **2019**, *141*, 15547–15556.
- (48) Bacellar, I. O. L.; Oliveira, M. C.; Dantas, L. S.; Costa, E. B.; Junqueira, H. C.; Martins, W. K.; Durantini, A. M.; Cosa, G.; Di Mascio, P.; Wainwright, M.; Miotto, R.; Cordeiro, R. M.; Miyamoto, S.; Baptista, M. S. Photosensitized Membrane Permeabilization Requires Contact-Dependent Reactions between Photosensitizer and Lipids. *J. Am. Chem. Soc.* **2018**, *140*, 9606–9615.
- (49) Yaremenko, I. A.; Vil', V. A.; Demchuk, D. V.; Terent'Ev, A. O. Rearrangements of Organic Peroxides and Related Processes. *Beil. J. Org. Chem.* **2016**, *12*, 1647–1748.
- (50) Davies, A. G. The Schenck Rearrangement of Allylic Hydroperoxides. *J. Chem. Res.* **2009**, 533–544.

- (51) Dang, H.-S.; Davies, A. G. Ene Reactions of Allylically Stannylated Cholestenes: Singlet Oxygenation of 7α -Triphenylstannylcholest-5-en-3β-Ol, and of 7α -Triphenylstannyl- and 7α -Tributylstannyl-cholest-5-ene-3-one, and the Rearrangement of 5α -Tributylstannylperoxy-3β-benzoyloxycholest-6-ne and of 7α -Tributylstannylperoxy-3β-benzoyloxycholest-5-ene. *J. Chem. Soc. Perkin Trans.* 2 **1992**, 7, 1095–1101.
- (52) Davies, A. G.; Davison, I. G. E. The Rearrangements of Allylic Hydroperoxides Derived from (+)-Valencene. *J. Chem. Soc. Perkin Trans.* 2 **1989**, No. 7, 825–830.
- (53) Lythgoe, B.; Trippett, S. Allylic Rearrangement of an Aβ-Unsaturated Hydroperoxide. *J. Chem. Soc.* **1959**, 471–472.
- (54) Griesbeck, A. G. Ene Reactions with Singlet Oxygen. In *CRC Handbook Org. Photochem. Photobiol.*; Horspool, W. M.; Song, P. S., Eds.; CRC Press: Boca Raton, 1995; pp 301–310.
- (55) Griesbeck, A. G.; Kleczka, M.; de Kiff, A.; Vollmer, M.; Eske, A.; Sillner, S. Singlet Oxygen and Natural Substrates: Functional Polyunsaturated Models for the Photooxidative Degradation of Carotenoids. *Pure Appl. Chem.* **2015**, *87*, 639–647.
- (56) Girotti, A. W.; Korytowski, W. Generation and Reactivity of Lipid Hydroperoxides in Biological Systems. *Chem. Peroxides* **2014**, *3*, 747–767.
- (57) Greene, L. E.; Lincoln, R.; Cosa, G. Rate of Lipid Peroxyl Radical Production during Cellular Homeostasis Unraveled via Fluorescence Imaging. *J. Am. Chem. Soc.* **2017**, *139*, 15801–15811.

- (58) Olson, A. S.; Jameson, A. J.; Kyasa, S. K.; Evans, B. W.; Dussault, P. H. Reductive Cleavage of Organic Peroxides by Iron and Thiols. *ACS Omega* **2018**, *3*, 14054–14063.
- (59) Girotti, A. W. Lipid hydroperoxide Generation, Turnover, and Effector Action in Biological Systems. *J. Lipid Res.* **1998**, *39*, 1529–1542.
- (60) O'Leary, W. M. Involvement of Methionine in Bacterial Lipid Synthesis. *J. Bacteriol.* **1959**, 78, 709–713.
- (61) Wang, Y.; Ferrer-Espada, R.; Baglo, Y.; Goh, X. S.; Held, K. D.; Grad, Y. H.; Gu, Y.; Gelfand, J. A.; Dai, T. Photoinactivation of Neisseria Gonorrhoeae: A Paradigm-Changing Approach for Combating Antibiotic-Resistant Gonococcal Infection. *J. Infect. Dis.* **2019**, *220*, 873–881.
- (62) Maytin, E. V.; Hasan, T. Vitamin D and Other Differentiation-Promoting Agents as Neoadjuvants for Photodynamic Therapy of Cancer. *Photochem. Photobiol.* **2020**, *96*, 529-538.
- (63) Maytin, E. V.; Anand, S.; Riha, M.; Lohser, S.; Tellez, A.; Ishak, R.; Karpinski, L.; Sot, J.; Hu, B.; Denisyuk, A.; Davis, S. C.; Kyei, A.; Vidimos, A. 5-Fluorouracil Enhances Protoporphyrin IX Accumulation and Lesion Clearance during Photodynamic Therapy of Actinic Keratoses: A Mechanism-Based Clinical Trial. *Clin. Cancer Res.* **2018**, *24*, 3026–3035.
- (64) Anand, S.; Rollakanti, K. R.; Brankov, N.; Brash, D. E.; Hasan, T.; Maytin, E. V. Fluorouracil Enhances Photodynamic Therapy of Squamous Cell Carcinoma via a p53-Independent Mechanism That Increases Protoporphyrin IX Levels and Tumor Cell Death. *Mol. Cancer Ther.* **2017**, *16*, 1092–1101.

- (65) Sinha, A. K.; Anand, S.; Ortel, B. J.; Chang, Y.; Mai, Z.; Hasan, T.; Maytin, E. V. Methotrexate Used in Combination with Aminolaevulinic Acid for Photodynamic Killing of Prostate Cancer Cells. *Br. J. Cancer* **2006**, *95*, 485–495.
- (66) Monro, S.; Colón, K. L.; Yin, H.; Roque J., III; Konda, P.; Gujar, S.; Thummel, R. P.; Lilge, L.; Cameron, C. G.; McFarland, S. A. Transition Metal Complexes and Photodynamic Therapy from a Tumor-Centered Approach: Challenges, Opportunities, and Highlights from the Development of TLD1433. *Chem. Rev.* **2019**, *119*, 797–828.
- (67) Dabrowski, J. M.; Pucelik, B.; Regiel-Futyra, A.; Brindell, M.; Mazuryk, O.; Kyziol, A.; Stochel, G.; Macyk, W.; Arnaut, L. G. Engineering of Relevant Photodynamic Processes Through Structural Modifications of Metallotetrapyrrolic Photosensitizers. *Coord. Chem. Rev.* **2016**, *325*, 67–101.
- (68) Durantini, A. M.; Greene, L. E.; Lincoln, R.; Martínez, S. R.; Cosa, G. Reactive Oxygen Species Mediated Activation of a Dormant Singlet Oxygen Photosensitizer: From Autocatalytic Singlet Oxygen Amplification to Chemicontrolled Photodynamic Therapy. *J. Am. Chem. Soc.* **2016**, *138*, 1215–1225.